Iron Dual-atom Catalyst combine with "vicinal nonmetallic sites" for efficient Ammonia Synthesis

Hongdan Zhu
Nankai University
Kairui Zhang
Nankai University
Jolyon Aarons
Nankai University
Qian Peng (qpeng@nankai.edu.cn)
Nankai University https://orcid.org/0000-0002-1218-5976

Article

Keywords: Brønsted–Evans–Polanyi Relation, Industrial Transformation, N2 Dissociation, B-N Lewis Pairs, Competitive Adsorption

Posted Date: March 22nd, 2021

DOI: https://doi.org/10.21203/rs.3.rs-319184/v1

Abstract

Ammonia synthesis from N2 under mild conditions is a long-term pursuit and goal, which theoretically limited by the Brønsted–Evans–Polanyi (BEP) relation in industrial transformation via the N2 dissociation. Here we show that the Fe2 catalyst combined with the “vicinal nonmetallic sites” may break the BEP limitation to fulfill the efficient ammonia synthesis. The catalyst supported on boron doped graphitic carbon nitride (Fe2/B/mpg-C3N4) strongly favors hydrogenation of *N2 to form a *NHNH2 species, which leads to low energy barriers for N-H formation (0.57eV) and N-N dissociation (0.51eV). Constructed B-N “Lewis pairs” on the mpg-C3N4 serve as nonmetallic sites can activate and transfer hydrogen, which reduce the competitive adsorption of N2 and H2. Through co-activated H2 on the vicinal site, synergistic Fe2 catalyst shows a significant advantage among Fen/mpg-C3N4 (n=2, 3, 4) catalysts and thus can avoid harsh reaction condition for the thermal conversion of N2 to NH3.

Introduction

Ammonia as a key precursor for nitrogenous fertilizers is crucial to ensure human survival and sustain the world’s population.[1] Currently, ammonia synthesis is dominated by the industrial Haber–Bosch (HB) process using heterogeneous iron-based catalysts.[2] Although this important catalytic reaction has been developed for a hundred years, it still requires harsh reaction conditions which are intensely energy dependent.[3, 4] Previous theoretical studies indicate that ammonia synthesis via the N_2 dissociative mechanism ($N_2+3H_2\rightarrow 2N+3H_2\rightarrow\rightarrow 2NH_3$) [5] abides by the Brønsted–Evans–Polanyi (BEP) relationship. [6-8] This implies the requirement for a moderate nitrogen adsorption strength on an applicable metal catalyst, enabling a compromise between N_2 dissociation and NH_x desorption. In 2017, the Chen group proposed that a LiH-mediated Fe surface breaks the BEP limitation for ammonia synthesis [9] (Scheme 1a). In biological nitrogen fixation processes, nitrogenase enzymes, containing FeMo, FeV, or FeFe cofactor, as catalytically active sites,[10] which are able to reduce N_2 at low temperatures and pressures probably proceeding by the associative mechanism of N_2 [11, 12] rather than the dissociative mechanism as in the HB process. [5] A similar catalytic reduction of N_2 under mild conditions was also proposed for electrochemical ammonia synthesis, based on theoretical studies.[13-15] However, there are still rare examples of ammonia synthesis via the associative mechanism in thermal catalysis ($N_2+3H_2\rightarrow N_2H+5/2H_2\rightarrow\rightarrow 2NH_3$), and the recent theoretical progress seems to indicate this associative mechanism in the catalytic reactions is underestimated.[16-19] Skúlason *et al*[17] suggested that a certain proportion of associative mechanism of N_2 on Ru(001) surfaces may reduce the N-N activation energy and lead to more efficient production of NH_3. Moreover, Li and coworkers revealed, through theoretical studies, that the associative hydrogenation mechanism has the potential to facilitate N_2 reduction by using small metal clusters as heterogeneous catalysts (Rh_1Co_3/CoO(011) or Fe_3/θ-Al_2O_3(010)) (Scheme 1a).[18,19] Even so, because the hydrogenation of nitrogen in the associative mechanism may not be facile,

the competition of the hydrogenation and N-N dissociation in NH_xNH_y(x=0-3, y=0-3) will become a key issue, which need to be solved for idea catalysts of ammonia synthesis. (Scheme 1b)

Binuclear iron is very important in biological enzymes, [20-26] such as [FeFe]-hydrogenase[20, 25,] and diiron monooxygenase,[21, 22] etc. In view of their superior performance in biology, binuclear iron complexes as mimic enzymes continue to intrigue interests, [27-33] especially for compounds used in N_2 activation.[29-33] Under the development of single-cluster catalysts, diatomic catalysts comprising the smallest type of metal clusters may provide a unique platform for bridging heterogeneous and homogeneous catalysis. [34, 35] Although diatomic catalysts remain a relatively obscure area, they have emerged with great potential for increasing catalytic performance.[34-37] Lu *et al* reported remarkable activity of Pt_2 dimers supported on graphene for hydrolytic dehydrogenation of ammonia borane, which is about 17 and 45 times more active than single Pt_1 sites and nanoparticles, respectively.[38] Moreover, both experiment and theory have proven that diatomic clusters were an effective catalyst in the electrochemical nitrogen reduction reaction (eNRR).[13, 39-42] However, the possible mechanisms on the diatomic clusters and their relationship with catalytic sites on single-cluster catalysts have not yet been revealed for the thermal conversion of N_2 to NH_3.

Recently, a series of highly dispersed dimer clusters supported on mesoporous carbon nitride (mpg-C_3N_4) have been successfully prepared and it has been demonstrated that the obtained Fe_2/mpg-C_3N_4 sample has superior catalytic performance for alkene epoxidation.[48] Because the "Fe_2N_4" structural center is similar to the low-coordinated iron complexes for the N_2 reduction, [44-46] diatomic iron models Fe_2/mpg-C_3N_4 were initially established to explore the high efficient catalyst for ammonia synthesis. In this work, we predict that Fe_2 diatomic catalyst strongly favors hydrogenation of $*N_2$ to form a $*NHNH_2$ species with the assistance of co-activated H_2 on the "vicinal nonmetallic sites", which leads to a low energy barrier for the N-N dissociation. In addition, the partial doping of boron on the carbon sites of the support was designed in Fe_2/B/mpg-C_3N_4 to overcome the relatively high energy barrier of the hydrogen transfer and promote the hydrogenation of nitrogen (Scheme 1b). We also further reveal that with increasing coordination number of Fe_n/mpg-C_3N_4 (n=2,3,4), the associative mechanism tended to be less competitive, and the dissociative mechanism became dominant in ammonia synthesis, which is controlled by the spin polarization of Fe_n. The Fe_2 cluster catalyst with its support strongly involved may provide an alternative perspective to bridge heterogeneous and homogeneous catalysis that bestows the potential for efficient ammonia synthesis.

Results

The "vicinal nonmetallic sites" -promoted Hydrogenation Mechanism

Inspired by the low-coordinated iron complexes of the "Fe_2N_4" for the N_2 reduction, [44-46] a diatomic catalyst, Fe_2/mpg-C_3N_4, was developed for the thermal conversion of N_2 to NH_3. The favorable configuration of Fe_2/mpg-C_3N_4 is shown in Figure 1a, where each Fe atom binds with two adjacent nitrogen atoms forming a flat-lying Fe_2 right above mesoporous graphitic carbon nitride. The binding energy of Fe_2 with mpg-C_3N_4 is thermodynamically stable at -7.53eV due to the back donation interactions of iron d orbitals to π* orbitals of the mpg-C_3N_4 support, substantiated by +1.08|e| Bader charges. The Fe_2 moiety is calculated with magnetic moment of 6μB. Such low oxidation state and high spin polarization characteristics on Fe_2 facilitate to activate N_2.[47]

Our investigation started with the adsorption of N_2 to understand the influence of the activation of nitrogen for the reaction mechanism. The adsorptions of N_2 on Fe_2/mpg-C_3N_4 were calculated in three models that were further verified by *Ab Initio* molecular dynamics (AIMD) simulations (Figure 1b and Figure S1-2). The most stable configuration is the side-on/side-on (μ-ŋ2:ŋ2) mode with E_{ads}= -1.52eV, which is different from the known "Fe-NN-Fe" complexes, [28, 29, 46,] probably due to the change in geometry impacting the Fe–NN-Fe bonding interaction. The calculated energies for side-on/end-on (μ-ŋ2:ŋ1) and terminal end-on (ŋ1:ŋ1) modes were 0.02 and 0.23eV less stable, respectively, see Table S1 for details. On close inspection of the μ-ŋ2:ŋ2 mode, the bond length of four Fe-N bonds varied from 1.92 to 1.98Å. The remarkably elongated N-N bond for chemisorbed N_2 (from 1.11 Å of free N_2 to 1.25 Å) can be ascribed to the back donation interactions of iron d orbitals to two π* orbitals of N_2, supported by the increase of negative charge (-0.86|e|) on the *N_2. Therefore, the μ-ŋ2:ŋ2 mode was used for the following mechanistic investigations of N_2 hydrogenation and N-N dissociation.[48]

Since the calculated N-N dissociative mechanism in Fe_2/mpg-C_3N_4 is particularly unfavorable via a 2.75eV energy barrier of N-N cleavage (Figure S3), the associative hydrogenation of N_2 will be an alternative choice. In contrast to the electro-catalytic reaction where protons and electrons are transferred directly to the adsorbed nitrogen, H_2 activation and transfer are important in the thermal catalytic hydrogenation of nitrogen. Due to lack of binding site on the Fe_2 cluster, H_2 molecules prefer to approach and absorb dissociatively on "C-N" site in the support rather than the Fe site with reaction energy -2.30eV versus -1.26eV, respectively (Figure 1c and Figure S4).[49, 50] The dissociation of H_2 tends to be hemolytic, to form C-H and N-H bonds, and the charges on each *H are 0.49|e| and 0.88|e|. Because of the H-H repulsion between the N1-H and N2-H, the activation of the second H_2 at the C1-N1 site (Figure 1c and Figure S4, E_{ads}= -2.18eV) is less stable. However, the H-H repulsion will make *H on the N1 site easily transfer to the Fe1 site with an energy barrier of 0.75eV. Then through an easily overcome 0.47eV energy barrier, this Fe1 bonded hydrogen (-0.17|e|) would attack the activated *N_2 and transfer its electrons to the π* orbital of *N_2 forming a *N_2H intermediate (a2-a4 in Figure 2a). Subsequently, the Fe1 site favors accepting the second *H on the C1 site by overcoming an activation energy barrier (E_a) of 1.38eV rather

than the *H on the N2 site (a4-a5, E_a=1.91eV), see Figure S5 for more details. The synergistic activation of H_2 at “vicinal nonmetallic sites” not only reduces the adsorption competition between N_2 and H_2, but also promotes the subsequent hydrogenation process of N_2 (A further discussion of hydrogen activation and transfer are in the last Section.).

After forming the *NNH intermediate (a5 in Figure 2), four different hydrogenation pathways are proposed to generate NH_3, dependent on different combinations of alternative/distal hydrogenation on $*N_2H$ and the N-N bond dissociation of $*NH_xNH_y$(x=0-3, y=0-3) intermediates (Figure 2 and Schematic depiction in Figure S6). It is favorable for *NNH to continue hydrogenation rather than to break the N-N bond due to the relatively high dissociation energy barrier (E_a=1.10eV in a5→d6, AH3). The following hydrogenation favors the formation of *HN-NH via an alternate hydrogenation (AH) mode with a 0.36eV energy barrier (a5→b6 in AH1), which is 0.30eV lower than the formation of $*N\text{-}NH_2$ via distal hydrogenation (DH) mode (a5→a6 in DH1). Then, the Fe1 site can accept and activate additional H_2 by breaking the Fe-N bond of *HN-NH to form co-adsorption configuration c7, which is ready to further transfer H* to nitrogen bonded to Fe2 site (c7→c8 via 0.36eV energy barrier in AH2). The resulting $*NHNH_2$ (c8) is unusual example in the thermal catalytic reaction, although it is very common in electro- and enzyme catalysis via the $N_2/H^+/e^-$ reaction system. [13, 39-41] With the continuous hydrogenation of $*N_2$ intermediates (a5→b6→c8), the N-N bond becomes much weaker and its bond length is elongated from 1.33 Å to 1.44 Å. The $*NHNH_2$ intermediate with an N–N single bond character ($_{stretch}$= 1007 cm^{-1}) would undergo N-N bond cleavage to form bridged μ-*NH and terminal $*NH_2$ as shown in c9 of Figure 2a. This N-N cleavage with 0.50eV energy barrier is facile and not a rate-limiting step, which is distinguished from direct cleavage of nitrogen in the Haber-Bosch process.[6, 7] Subsequently, the remaining H* on the Fe1 center is further transferred to the μ-*NH forming the $\mu\text{-}*NH_2$ species. The last H_2 would still be activated by the Fe1 center, and delivers the active H* species to generate two NH_3. Since the hydrogenation mechanism of nitrogen in Fe_2/mpg-C_3N_4 relies on synergistic catalysis of Fe_2 active sites and “vicinal nonmetallic sites”, we call it “vicinal nonmetallic sites” promoted hydrogenation mechanism. The key intermediates of the preferred reaction pathway are illustrated in Figure S7. More details for four reaction pathways such as optimized intermediates, transition states and energy diagrams are also given in Figure S8-11.

In fact, the reaction pathways calculated above mainly include two types of reactions: N-N bond dissociation and N-H bond formation. Energy barriers for N-N bond dissociations will significantly decrease depending on the gradual hydrogenations to form different $*NH_xNH_y$ (N-NH, NH-NH, $N\text{-}NH_2$ and $NH\text{-}NH_2$) intermediates in Figure 2b. This can be rationalized by electron accumulations on related $*N_2$ and elongated N-N bond lengths during the hydrogenation (Table S2). Therefore, promoting the hydrogenation of $*N_2$ would be an applicable way to lower the energy barrier of N-N dissociation. As

shown in Figure 3, the complicated N-H bonds formation reactions in different pathways can be resolved to two kinds according to whether the N-N bond is dissociated or not. The nitrogen hydrogenation energy barriers on Fe_2 clusters are low and vary from 0.22 to 0.66eV, probably due to the electronic structures of $*N_2$ and the proper Fe-H bond strength. In addition, it is more feasible for the Fe_2 cluster with low positive Bader charges to transfer their hydrogen (e.g. a11-a12/c9-c10 or a8-a9/b11-a12, etc. in Figure 3). Overall, Fe_2/mpg-C_3N_4 could be a potential catalyst for N_2-to-NH_3 conversion with a lower hydrogenation barrier (0.36eV in TS-a5-b6 and 0.36eV in TS-c7-c8) and a lower N-N bond dissociation barrier (0.50eV in TS-c8-c9) in the AH2 reaction pathway.

The Mechanisms of Nitrogen Reduction on various Iron clusters

As diverse multinuclear systems in active sites can significantly change the adsorption mechanism and catalytic performance, we preformed more mechanistic studies of nitrogen reduction by using the newly designed Fe_3/mpg-C_3N_4, [51] Fe_4/mpg-C_3N_4 and the Fe (211) surface[19] for the comparisons with the Fe_2/mpg-C_3N_4 system. The reaction pathways and corresponding structures can be obtained in Figure S12-S13. Catalytic N-H bond formation and N-N bond dissociation as key reaction steps are illustrated in Figure 4 to probe the relationship between mechanisms and iron coordination numbers (Fe_n) of the adsorption sites. [52] Generally, the coordination numbers of the iron active sites have the opposite correlation with the energy barriers of N-N bond breakage (Figure 4a) and N-H bond formation (Figure 4b), as seen in the negative and positive slopes of the linear relationships, respectively. With the increase of coordination number of irons, N-N bond dissociation barriers of $*NH_xNH_y$ (x=0-1, y=0-2) gradually decrease, while the energy barriers for N-H bond formation of $*NH_xNH_y$ (x=0-1, y=0-2) tend to be unfavorable. Furthermore, with increasing hydrogen atoms in $*NH_xNH_y$ (x=0-1, y=0-2) in the linear relation diagram, the N-N bond breaking energy barrier seems to be less sensitive to the Fe coordination number, which is supported by the flattening slope. That is in contrast to N-H bond formation with positive correlation. These findings intrigued us to further investigate the mechanistic details of the N_2-to-NH_3 thermal conversion.

As shown in Figure 5 and Figure S14, key reaction pathways of related iron clusters indicate the Fe_3/mpg-C_3N_4 and Fe_4/g-C_3N_4 systems tend to form *NNH via $*N_2$ hydrogenation (0.95eV in Fe_3/mpg-C_3N_4 and 1.32eV in Fe_4/mpg-C_3N_4), followed by N-NH bond cleavage with energy barriers of 0.69eV and 0.31eV respectively. The continued hydrogenations to form *NH-NH or $*N-NH_2$ were unfavorable due to high energy barrier (Figure S12-13). These mechanistic results in Fe_n/mpg-C_3N_4(n=3,4) are consistent with results in Fe_3/Al_2O_3 clusters from Li's group.[19] There might be an energy crossover point in the Fe_4/mpg-C_3N_4, because the energy barriers of N-N bond cleavage (1.34eV) and N-H bond formation (1.32eV) are quite close, indicating that Fe coordination number over four will cause the dissociative mechanism of nitrogen to dominate. For example, the energy barrier for the direct dissociation of the N_2 molecule is only

0.50eV at the Fe (211) C7 site.[19] On the contrary, the Fe_2/mpg-C_3N_4 catalyzed system favors continuous hydrogenation of *NNH until the formation of *$NHNH_2$, which can promote the breaking of the N-N bond. Such a synergistic associative mechanism can break the traditional BEP relationship with low N-N dissociation energy barrier and low NH_x adsorption energy compared with metal surfaces [53, 54] such as Figure 5b. We can rationalize the results through charges of *N_2 as shown in their relationship with energy barriers of N-N dissociation and N-H formation (Figure 5c). With more coordination of Fe_n, the negative charges of *N_2 will increase that enable N-N bond cleavage to be facile, but inhibit *N_2 hydrogenation via Fe-hydride intermediates. Therefore, the fewer electrons on nitrogen, the more favorable it is for the hydride to transfer hydrogen to adsorbed *NH_xNH_y (x=0-1, y=0-2) on the iron sites.

Electronic structure analysis

Besides the Bader charge analysis, projected density of states (PDOS) of adsorbed N_2 on different clusters can provide further explanation. As shown in Figure 6a, the α-spin orbitals of the Fe_2 clusters are much lower energy than the 2π* orbitals of N_2, which cannot fulfill the orbital interaction. The well matched β-spin d orbital of Fe_2 can partially donate its electron to the 2π*orbital of N_2 forming a β-spin d-π* interaction, which leads to the strong spin polarization of the *N_2. This result was further supported by differential charge density and spin density (Figure 6b). Through fragment orbital analysis between an isolated Fe_2 cluster and N_2 in Figure 6c and Figure S15, the occupied β-d_{xy-xy}/β-d_{xz-xz} orbitals of the Fe_2 species can interact with empty nitrogen 2π* orbitals to form two bonding orbitals (β-d_{xy-xy}+π* and β-d_{xz-xz}+π*), which is consistent with molecular orbital interaction between nitrogen and Fe_2/mpg-C_3N_4 (Figure S16) and indicate the electron transfer from Fe_2 to nitrogen. Therefore the strong spin polarization of the activated *N_2 will facilitate to accept the electron and therefore make hydrogen transfer process on the metal-hydride accessible. In terms of the Fe coordination number increase (Figure 6a), the α-spin orbitals of Fe_n clusters have shifted to relatively high energy levels and match with the energy level of the 2π* orbitals of N_2. The additional electron transfer from α-spin orbitals of Fe clusters will lead to an increase in the electron and a decrease in the spin polarization for *N_2, further weakening of the bond strength of *N_2, which promotes the N-N bond dissociation. When the coordination numbers of Fe is over 4, such as C7 site of Fe (211), the energy barrier for direct cleavage of N-N bond is favorable. For Fe_n/g-C_3N_4 (n=2,3) catalysts, the N_2 associative mechanism becomes dominant in nitrogen reduction to ammonia, supported by previous discussion in Figures 4 and 5.

To understand the unusual hydrogenation mechanism of N_2 on the smallest cluster-Fe_2/mpg-C_3N_4, the projected density of states (PDOS) and spin densities for key intermediates were shown in Figure 7. With continuous hydrogenation, both Fe_2 clusters and the absorbed hydrogens transfer their electrons to the

N_2 2π* orbitals, which decreased the energy of the N-N anti-bond orbital and activates the N-N bond in Figure 7a. The formed *NNH has relatively high spin polarization to make the next hydrogenation favorable, forming *NHNH via an alternate pathway. Because the α-spin electrons of the N_2 2π*orbital keep increasing from *NN to *$NHNH_2$, the spin density for each intermediate is gradually eroded until *$NHNH_2$ with no obvious spin density. After that, the following transformation would favor the dissociation of the N-N bond rather than additional hydrogenation. In contrast, the spin density of *NNH in Fe_3/g-C_3N_4 is relatively low, hindering further hydrogenation and making N-N bond cleavage accessible.

The efficient catalyst by B doping mpg-C3N4

Although the iron diatomic cluster shows a catalytic advantage in the synergistic associative mechanism for ammonia synthesis, the hydrogen transfer from the C1 site of the mpg-C_3N_4 support to Fe active sites seems unfavorable (E_a(C-H) = 1.38eV in a4 a5 of Figure 8a and Figure 2), which might severely hinder the following transformation. To accelerate this step, we tried to modulate hydrogen adsorption by doping other heteroatoms (including B, O, and N) at the C1 site as shown in Figure S17 and Figure 8. Theoretical simulation indicates that doping with B atoms would not only maintain the stability of the structure, but also promote the activation and conversion of H_2.

In B-doped Fe_2/mpg-C_3N_4 (Fe_2/B/mpg-C_3N_4), two H_2 molecules were absorbed dissociatively on the C-N and B-N sites with adsorption energy of -2.33eV (a2 in Figure 8b). Different from the C-N site on the support, the dissociation of H_2 in the B-N site tends to be heterolysis forming B-H^- and N-H^+ that are supported by the -0.57|e| and +0.45|e| charges on hydrogens, respectively. The *H stabilized by the electron-deficient B atom (as Lewis acid) will change the transfer order of *H on supports acting as a non-innocent ligand in homogenous catalysis. [55, 56] In the Fe_2/B/mpg-C_3N_4, *H on the B site would preferentially transfer to the Fe1 site with an energy barrier of 0.75eV and continue to attack the activated *N_2 to form the *N_2H intermediate. After that, the *H on the N1 site will shift to the Fe1 site via a 0.86eV barrier that is slightly higher energy compared to that in the Fe_2/mpg-C_3N_4 system (0.75eV). However, the overall hydrogen transfer process by doping the support with B would reduce the energy barrier from 1.38eV to 0.86eV. This designed B-N system can be regarded as a typical “Lewis pair” that enables heterolysis of the H-H bond and facilitates the hydrogen transfer.[57]

Stimulated by the excellent theoretical performance of Fe_2/B/mpg-C_3N_4 for H_2 activation and transformation, we recalculated the nitrogen reduction mechanism to further investigate whether doping with B will affect the conversion of N_2. As shown in Figure S18 and Figure 9a, the doping of B atoms

does not change the reaction mechanism, and the variation of energy barriers for the subsequent N_2 reduction reaction can be ignored (±0.02eV). Therefore, B doping of the support was selectively targeted to optimize of the H transfer process without hampering other catalytic processes, it would be a good candidate to improve the catalytic performance of N_2 reduction. Furthermore, Microkinetic analysis of Fe_2/mpg-C_3N_4 and Fe_2/B/mpg-C_3N_4 by the rate determining states method, proposed by Kozuch *et al*, [58] are conducted to further probe the reaction rate for the influence of B doping and the catalytic performance. The calculated TOF of ammonia synthesis on Fe_2/B/mpg-C_3N_4 is 6.34×10^{-1} s^{-1} $site^{-1}$ at 100 bar and 700 K, which is 2 orders of magnitude faster than the reaction rate of Fe_2/mpg-C_3N_4 (3.07×10^{-3} s^{-1} $site^{-1}$). The TOF of ammonia production on Fe_2/B/mpg-C_3N_4 is less than 10^{-10} s^{-1} $site^{-1}$ below 400 K, which is due to the stable NH_x adsorption species at low temperature. Due to entropy effects for free gases, the bare site will increase accordingly after desorption of NH_x upon the temperature rise. Under the condition of constant pressure, the temperature increased from 300K to 700K, and the reaction rate increased by 13-14 orders of magnitude. At constant 700K temperature, the pressure has a relatively gentle effect on the reaction rate, so it is expected to realize the nitrogen conversion reaction at low pressure (Figure 9d in Fe_2/B/g-C_3N_4). In order to achieve maximum TOF, our calculated partial pressure of N_2 is 0.3 ($P_{N2}/P_{(N2+H2)}$), close to ideal ratio of 1/4 (Figure 9c), indicating that the Fe_2/B/g-C_3N_4 catalyst can reduce the competitive adsorption of N_2 and H_2. That is distinct from Fe_3/Al_2O_3 forming the co-adsorption of N_2 and H_2 on Fe_3 clusters, which leads to a 0.44 partial pressure of N_2 for maximum TOF. In contrast, it is necessary to remarkably change the partial pressure of nitrogen in classical metal catalysts, for example 0.06 ($P_{N2}/P_{(N2+H2)}$) in the Fe (211) C7 site and 0.78 in the Ru (001) B5 site. [19]

Discussion

In conclusion, we have revealed that, with the decrease of coordination number in Fe_n/mpg-C_3N_4 (n=4, 3, 2), the hydrogenation mechanism tends to be dominant, and the dissociative mechanism is no longer favored for ammonia synthesis, which is controlled by the spin polarization of Fe_n. The mechanism is conducive to the continuous hydrogenation of $*N_2$ on the Fe_2 cluster owing to the highest energy gap of spin d-orbitals in Fe_n/mpg-C_3N_4 (n=4, 3, 2), mimicking the nitrogen fixation process in biological nitrogenase. The N-N bond can be activated by the continuous hydrogenation of $*N_2$ because of the increasing electron occupancy of the N_2's 2π* orbitals and the decreasing energy of the N-N anti-bond orbital.

As shown in Figure 10, we propose that iron diatomic clusters anchored on boron doped mpg-C_3N_4 (Fe_2/B/mpg-C_3N_4) can achieve efficient thermal conversion of N_2 to NH_3 by a "vicinal nonmetallic sites"-promoted hydrogenation mechanism. This reaction pathway mainly includes the activation and transfer of H_2, the formation of $NHNH_2$, the N-N bond break and the formation of ammonia. The $*N_2$ can be hydrogenated to form $*NHNH_2$, leading to a low energy barrier (0.51eV) in the N-N bond dissociation. By partially doping boron on the carbon site of the support, the mpg-C_3N_4 support can act as a mimic non-

innocent ligand of homogenous catalysts to activate and transfer hydrogen (the rate determining step of the hydrogen transfer energy barrier was reduced form 1.38eV in mpg-C_3N_4 to 0.86eV in B/mpg-C_3N_4), which reduces the competitive adsorption of N_2 and H_2. And then, the synergistic effect of Fe_2 and "vicinal nonmetallic sites" of mpg-C_3N_4 achieves the most favorable hydrogenation pathway for thermal conversion of N_2 to NH_3.

Notably, the Fe_2/B/mpg-C_3N_4 catalyst with synergistic hydrogenation mechanism in the combined advantages of traditional thermal catalysis and electro-catalysis in ammonia synthesis, which not only breaks the BEP limitation of metal surface catalysts, but also avoids competitive reactions in electro-catalysis. Through theoretical calculations, we propose that the synergistic effect of Fe_2 and "vicinal nonmetallic sites" of mpg-C_3N_4 may lead to better catalytic performance for the idea thermal conversion of N_2 to NH_3. The current Fe_2 catalyst model may still be improved, however, diatomic catalysts with high spin polarization are expected to be used to activate and transform more inert molecules. Modifying the support based on "Lewis pair" is an effective method and provides a distinct strategy for the development of more efficient catalysts.

Methods

The computations were performed with the spin-polarized density functional theory (DFT) method, as implemented in the Vienna *ab initio* Simulation Package (VASP version 5.4.4).[59] The exchange correlation energy was modeled with the Perdew–Burke–Ernzerhof (PBE) functional [60] within the generalized gradient approximation (GGA). For models of Fe_n/mpg-C_3N_4 (n=2,3,4) and Fe_2/B/mpg-C_3N_4, we chose 2×2 supercell of C_3N_4 and the Brillouin zone was sampled by 2 × 2 × 1 k-points using the Monkhorst–Pack scheme in structural optimizations. An energy cutoff of 500eV was adopted for the plane-wave basis. To avoid interactions between repeated images, a vacuum gap of 15 Å was used in the direction perpendicular to the 2D layer. The energy and force convergence thresholds for the iterations in the self-consistent field (SCF) were set to 10^{-5} eV and 0.02 eV/Å, respectively. The transition states were obtained by climbing image nudged elastic-band method (CI-NEB) [61] combined with the Dimer [62] method and further confirmed by vibrational frequency analysis.

Fragment Molecular orbitals (FMOs) analyses were performed using spin-unrestricted DFT with the PBE exchange-correlation functional and DZP Slater basis sets as implemented in the Amsterdam Density Functional (ADF 2019. 304) program. [63] The scalar relativistic (SR) effect was included by the zero-order-regular approximation (ZORA).[64] At the same time, spin multiplicity calculations for Fe_2/mpg-C_3N_4 and N_2 adsorption in Table S3-4 and partial molecular orbitals (MOs) of N_2 adsorption configuration in Figure S16 were performed with the ω-B97XD functional [65] and def2SVP basis sets as implemented in Gaussian 09, [66] which also proved the high spin polarization of Fe_2/mpg-C_3N_4.

Declarations

Acknowledgments

We gratefully acknowledge the National Natural Science Foundation of China (21890722, 21950410519, 21702109,), the Natural Science Foundation of Tianjin Municipality (19JCJQJC62300, 18JCYBJC21400), Tianjin Research Innovation Project for Postgraduate Students (2019YJSB081) and the Fundamental Research Funds for Central Universities [Nankai University (No. 63201043)] for generous financial support.

Author contributions

Q.P. conceived and directed the research. H.-D. Z. conceived and performed all the calculations. Q.P. and H.-D. Z. co-wrote the paper. All the authors discussed the results and commented on the manuscript

Additional information.

Additional comments and discussion of the findings in the paper, and supplemental data (PDF)

Competing interests

The authors declare no competing interests.

References

1. Galloway, J. N. et al. Transformation of the Nitrogen Cycle: Recent Trends, Questions, and Potential Solutions. *Science* **320**, 889-892 (2008).
2. Liu, H. Ammonia synthesis catalyst 100 years: practice, enlightenment and challenge. *Chinese J. Catal.* **35**, 1619-1640 (2014).
3. Yoshiaki, T. & Yoshiaki, N. Developing more sustainable processes for ammonia synthesis. *Coordination Chemistry Reviews* **257**, 2551– 2564 (2013).
4. Giddey, S., Badwal, S. P. S., Munnings, C. & Dolan, M. Ammonia as a Renewable Energy Transportation Media. *ACS Sustainable Chem. Eng.* **5**, 10231−10239 (2017).
5. Rod, T. H., Logadottir, A. & Nørskov, J. K. Ammonia synthesis at low temperatures. *J. Chem. Phys.* **112**, 5343-5347 (2000).
6. Zhang, C., Liu, Z.-P. & Hu, P. Stepwise addition reactions in ammonia synthesis: A first principles study. *J. Chem. Phys.* **115**, 609-611 (2001).
7. Mortensen, J. J., Morikawa, Y., Hammer, B., & Nørskov, J. K. Density Functional Calculations of N_2 Adsorption and Dissociation on a Ru(0001) Surface. *J. Catal.* **169**, 85–92 (1997).
8. Medford, A. J. et al. From the Sabatier principle to a predictive theory of transition-metal heterogeneous catalysis. *J. Catal.* **328**, 36-42 (2015).
9. Wang, P. et al. Breaking scaling relations to achieve low-temperature ammonia synthesis through LiH-mediated nitrogen transfer and hydrogenation. *Nat. Chem.* **9**, 64-70 (2017).

10. Barbara, K. B., & David, J. L. Mechanism of Molybdenum Nitrogenase. *Chem. Rev.* **96**, 2983–3011 (1996).
11. Rod, T. H. & Nørskov, J. K. Modeling the Nitrogenase FeMo Cofactor. *J. Am. Chem. Soc.* **122**, 12751-12763 (2000).
12. Hoffman, B. M., Dean, R. D. & Seefeldt, L. C. Climbing Nitrogenase: Toward a Mechanism of Enzymatic Nitrogen Fixation. *Acc. Chem. Res.* **42**, 609-619 (2009).
13. Guo, X., Gu, J., Lin, S., Zhang, S., Chen, Z. & Huang, S. Tackling the Activity and Selectivity Challenges of Electrocatalysts toward the Nitrogen Reduction Reaction via Atomically Dispersed Biatom Catalysts. *J. Am. Chem. Soc.* **142**, 5709-5721 (2020).
14. Liu, X., Jiao, Y., Zheng, Y., Jaroniec, M. & Qiao, S. Z. Building Up a Picture of the Electrocatalytic Nitrogen Reduction Activity of Transition Metal Single-Atom Catalysts. *J .Am. Chem. Soc.* **141**, 9664-9672 (2019).
15. Tang, S., Dang, Q., Liu, T., Zhang, S., & Jiang, J. Realizing a not-strong-not-weak polarization electric field in single-atom catalysts sandwiched by boron nitride and graphene sheets for efficient nitrogen fixation. *J. Am. Chem. Soc.* **142**, 19308-19315 (2020).
16. Zeinalipour-Yazdi, C. D., Hargreaves, J. S. J. & Catlow, C. R. A. Low-T Mechanisms of Ammonia Synthesis on Co_3Mo_3N. *J. Phys. Chem. C* **122**, 6078-6082 (2018).
17. Garden, A. L. & Skúlason, E. The Mechanism of Industrial Ammonia Synthesis Revisited: Calculations of the Role of the Associative Mechanism. *J. Phys. Chem. C* **119**, 26554-26559 (2015).
18. Ma, X. L., Liu, J. C., Xiao, H. & Li, J. Surface Single-Cluster Catalyst for N_2-to-NH_3 Thermal Conversion. *J. Am. Chem. Soc.* **140**, 46-49 (2018).
19. Liu, J. C., Ma, X. L., Li, Y., Wang, Y. G., Xiao, H. & Li, J. Heterogeneous Fe_3 single-cluster catalyst for ammonia synthesis via an associative mechanism. *Nat. Commun.* **9**, 1610 (2018).
20. Chongdar, N. et al Unique Spectroscopic Properties of the H-Cluster in a Putative Sensory [FeFe] Hydrogenase. *J. Am. Chem. Soc.* **140**, 1057-1068 (2018).
21. Lee, S. K., Fox, B. G., Frolard, W. A., Lipscomb, J. D. & Münck, E. A Transient Intermediate of the Methane Monooxygenase Catalytic Cycle Containing an FeIVFeIV Ouster. *J. Am. Chem. Soc.* **115**, 6450-6451 (1993).
22. Dong, L. B. et al. Characterization and Crystal Structure of a Nonheme Diiron Monooxygenase Involved in Platensimycin and Platencin Biosynthesis. *J. Am. Chem. Soc.* **141**, 12406-12412 (2019).
23. Manley, O. M., Fan, R., Guo, Y. & Makris, T. M. Oxidative Decarboxylase UndA Utilizes a Dinuclear Iron Cofactor. *J. Am. Chem. Soc.* **141**, 8684-8688 (2019).
24. Park, K. et al. Peroxide Activation for Electrophilic Reactivity by the Binuclear Non-heme Iron Enzyme AurF. *J. Am. Chem. Soc.* **139**, 7062-7070 (2017).
25. Britt, R. D., Rao, G. & Tao, L. Bioassembly of complex iron–sulfur enzymes: hydrogenases and nitrogenases. *Nat. Rev. Chem.* (2020).

26. Frey, A. G. et al. Iron chaperones PCBP1 and PCBP2 mediate the metallation of the dinuclear iron enzyme deoxyhypusine hydroxylase. *PNAS* **111**, 8031-8036 (2014).
27. Wang, L. et al. O_2 Activation by Non-Heme Thiolate-Based Dinuclear Fe Complexes. *Inorg. Chem.* **59**, 3249-3259 (2020).
28. Zhang, S. et al. N-H Bond Formation at a Diiron Bridging Nitride. *Angew. Chem. Int. Ed.* **59**, 15215–15219 (2020).
29. Liu, T., Gau, M. R. & Tomson, N. C. Mimicking the Constrained Geometry of a Nitrogen-Fixation Intermediate. *J. Am. Chem. Soc.* **142**, 8142-8146 (2020).
30. Wasada-Tsutsui, Y. et al. Efficient Electronic Structure to Stabilize N_2-Bridged Dinuclear Complexes Intended for N_2 Activation: Iminophosphorane Iron(I) and Cobalt(I). *Eur. J. Inorg. Chem.* **2020**, 1411-1417 (2020).
31. Sorsche, D. et al. Unusual Dinitrogen Binding and Electron Storage in Dinuclear Iron Complexes. *J. Am. Chem. Soc.* **142**, 8147-8159 (2020).
32. McWilliams, S. F., Rodgers, K. R., Lukat-Rodgers, G., Mercado, B. Q., Grubel, K. & Holland, P. L. Alkali Metal Variation and Twisting of the FeNNFe Core in Bridging Diiron Dinitrogen Complexes. *Inorg. Chem.* **55**, 2960-2968 (2016).
33. Gu, N. X., Oyala, P. H. & Peters, J. C. An S = (1)/2 Iron Complex Featuring N_2, Thiolate, and Hydride Ligands: Reductive Elimination of H_2 and Relevant Thermochemical Fe-H Parameters. *J. Am. Chem. Soc.* **140**, 6374-6382 (2018).
34. Pan, Y., Zhang, C., Liu, Z., Chen, C. & Li, Y. Structural Regulation with Atomic-Level Precision: From Single-Atomic Site to Diatomic and Atomic Interface Catalysis. *Matter* **2**, 78-110 (2020).
35. Zhang, J., Huang, Q.-a., Wang, J., Wang, J., Zhang, J. & Zhao, Y. Supported dual-atom catalysts: Preparation, characterization, and potential applications. *Chinese J. Catal.* **41**, 783-798 (2020).
36. Li, Z., Ji, S., Liu, Y., Cao, X., Tian, S., Chen, Y., Niu, Z. & Li, Y. Well-Defined Materials for Heterogeneous Catalysis: From Nanoparticles to Isolated Single-Atom Sites. *Chem. Rev.* **120**, 623-682 (2020).
37. Chen, Z. W., Chen, L. X., Yang, C. C. & Jiang, Q. Atomic (single, double, and triple atoms) catalysis: frontiers, opportunities, and challenges. *J. Mater. Chem. A* **7**, 3492-3515 (2019).
38. Yan, H. et al. Bottom-up precise synthesis of stable platinum dimers on graphene. *Nat. Commun.* **8**, 1070 (2017).
39. Zheng, X., Yao, Y., Wang, Y., Liu & Y. J. N. Tuning the electronic structure of transition metals embedded in nitrogen-doped graphene for electrocatalytic nitrogen reduction: a first-principles study. *Nanoscale* **12**, 9696-9707 (2020).
40. Zhang, H., Cui, C. & Luo, Z. MoS_2-Supported Fe_2 Clusters Catalyzing Nitrogen Reduction Reaction to Produce Ammonia. *J. Phys. Chem. C* **124**, 6260-6266 (2020).
41. Li, Y., Zhang, Q., Li, C., Fan, H.-N., Luo, W.-B., Liu, H.-K. & Dou, S.-X. Atomically dispersed metal dimer species with selective catalytic activity for nitrogen electrochemical reduction. *J. Mater. Chem. A* **7**, 22242-22247 (2019).

42. He, T., Puente Santiago, A. R. & Du, A. Atomically embedded asymmetrical dual-metal dimers on N-doped graphene for ultra-efficient nitrogen reduction reaction. *J. Catal.* **388**, 77-83 (2020).
43. Tian, S. et al. Carbon nitride supported Fe_2 cluster catalysts with superior performance for alkene epoxidation. *Nat. Commun.* **9**, 2353 (2018).
44. Smith, J. M. et al. Stepwise reduction of dinitrogen bond order by a low-coordinate iron complex. *J. Am. Chem. Soc.* **123**, 9222–9223 (2001).
45. Smith, J. M. et al. Studies of low-coordinate iron dinitrogen complexes. *J. Am. Chem. Soc.* **128**, 756-769 (2006).
46. Pollock, C. J., Grubel, K., Holland, P. L. & Debeer, S. Experimentally quantifying small-molecule bond activation using valence-to-core X-ray emission spectroscopy. *J. Am. Chem. Soc.* **135**, 11803-11808 (2013).
47. Mcwilliams, S. F. & Holland, P. L. Dinitrogen Binding and Cleavage by Multinuclear Iron Complexes. *Acc. Chem. Res.* **46**, 2059-2065 (2015).
48. Li, X. F. et al. Conversion of Dinitrogen to Ammonia by FeN3-Embedded Graphene. *J. Am. Chem. Soc.* **138**, 8706-9 (2016).
49. Wei, S. et al. Direct observation of noble metal nanoparticles transforming to thermally stable single atoms. *Nat Nanotechnol* **13**, 856-861 (2018).
50. Vile, G., Albani, D., Nachtegaal, M., Chen, Z., Dontsova, D., Antonietti, M., Lopez, N. & Perez-Ramirez, J. A stable single-site palladium catalyst for hydrogenations. *Angew. Chem. Int. Ed.* **54**, 11265- 11269 (2015).
51. Wang, X. et al. Confined Fe-Cu Clusters as Sub-Nanometer Reactors for Efficiently Regulating the Electrochemical Nitrogen Reduction Reaction. *Adv. Mater.* **32**, 2004382 (2020).
52. Calle-Vallejo, F., Loffreda, D., Koper, M. T. & Sautet, P. Introducing structural sensitivity into adsorption-energy scaling relations by means of coordination numbers. *Nat. Chem.* **7**, 403-410 (2015).
53. Hummelshoj, J. S., Abild-Pedersen, F., Studt, F., Bligaard, T. & Norskov, J. K. CatApp: a web application for surface chemistry and heterogeneous catalysis. *Angew. Chem. Int. Ed.* **51**, 272-274 (2012).
54. https://slac.stanford.edu/~strabo/catapp/CatApp.html.
55. Liu, Y.-C., Yen, T.-H., Chu, K.-T. & Chiang, M.-H. Utilization of Non-Innocent Redox Ligands in [FeFe] Hydrogenase Modeling for Hydrogen Production. *Comments on Inorganic Chemistry* **36**, 141-181 (2015).
56. Kireev, N. V. et al. Bis[diphenylphosphino]methane and its bridge-substituted analogues as chemically non-innocent ligands for H_2 activation. *Chem. Commun.* **56**, 2139-2142 (2020).
57. Jiang, C., Blacque, O., Fox, T. & Berke, H. Heterolytic Cleavage of H_2 by Frustrated B/N Lewis Pairs. *Organometallics* **30**, 2117-2124 (2011).
58. Sebastian, K. & Sason S. How to Conceptualize Catalytic Cycles? The Energetic Span Model. *Acc. Chem. Res.* **44**, 101–110 (2011).

59. Kresse, G., Efficient iterative schemes for Ab Initio total-energy calculations using a plane-wave basis set. *Phys. Rev. B* **54**, 11169-11186 (1996).
60. Perdew, J. P., Burke, K. & Ernzerhof, M. Generalized Gradient Approximation Made Simple. *Phys. Rev. Lett.* **77**, 3865-3868 (1996).
61. Henkelman, G., Uberuaga, B. P. & Jonsson, H. A climbing image nudged elastic band method for finding saddle points and minimum energy paths. *J. Chem. Phys.* **113**, 9901-9904 (2000).
62. Henkelman, G. & Jónsson, H. A dimer method for finding saddle points on high dimensional potential surfaces using only first derivatives. *J. Chem. Phys.* **111**, 7010-7022 (1999).
63. Velde, G. T., Bickelhaupt, F. M., Baerends, E. J., Guerra, C. F., Vangisbergen, S. J. A., Snijders, J. G. & Ziegler, T. Chemistry with ADF. *J. Comput. Chem.* **22**, 931–967 (2001).
64. Lenthe, E.V., Baerends, E. J. & Snijders, J. G. Relativistic regular two-component Hamiltonians. *J. Chem. Phys.* **99**, (1996).
65. Chai, J. D. & Head-Gordon, M. Long-range corrected hybrid density functionals with damped atom-atom dispersion corrections. *Phys. Chem. Chem. Phys.* **10**, 6615-6620 (2008).
66. Gaussian, R.et al. Gaussian, Gaussian, Inc., Wallingford, CT. *Gaussian, Inc., Wallingford CT* (2004).

Figures

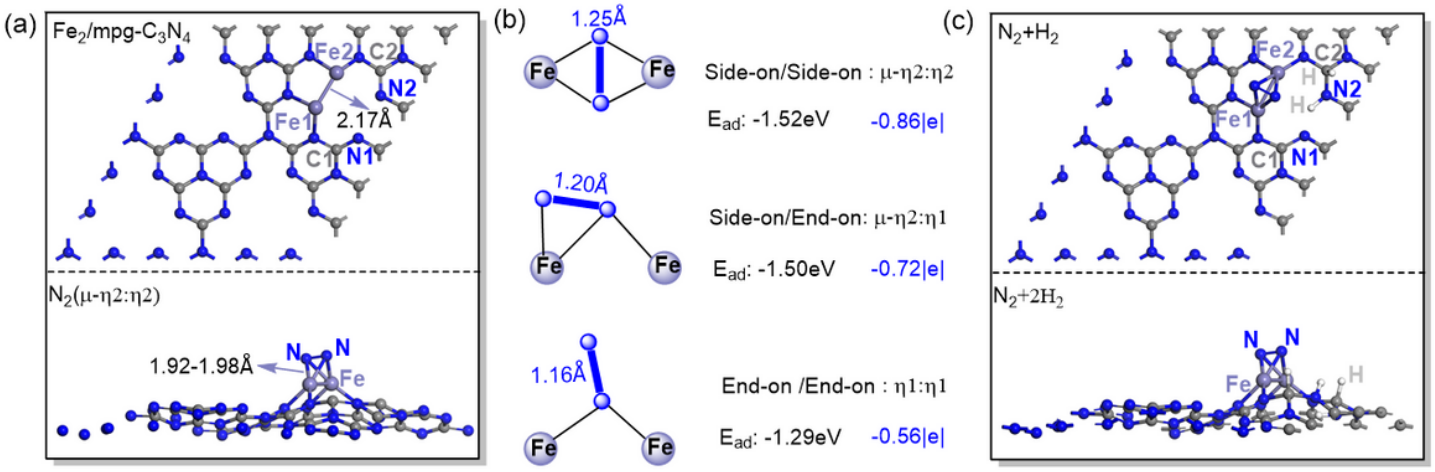

Figure 1

(a) The most stable Fe2/mpg-C3N4 cluster and nitrogen adsorption configuration; (b) Simplified adsorption forms of N2, N-N distance and its Bader charge were shown in blue; (c) The most stable co-adsorption configuration.

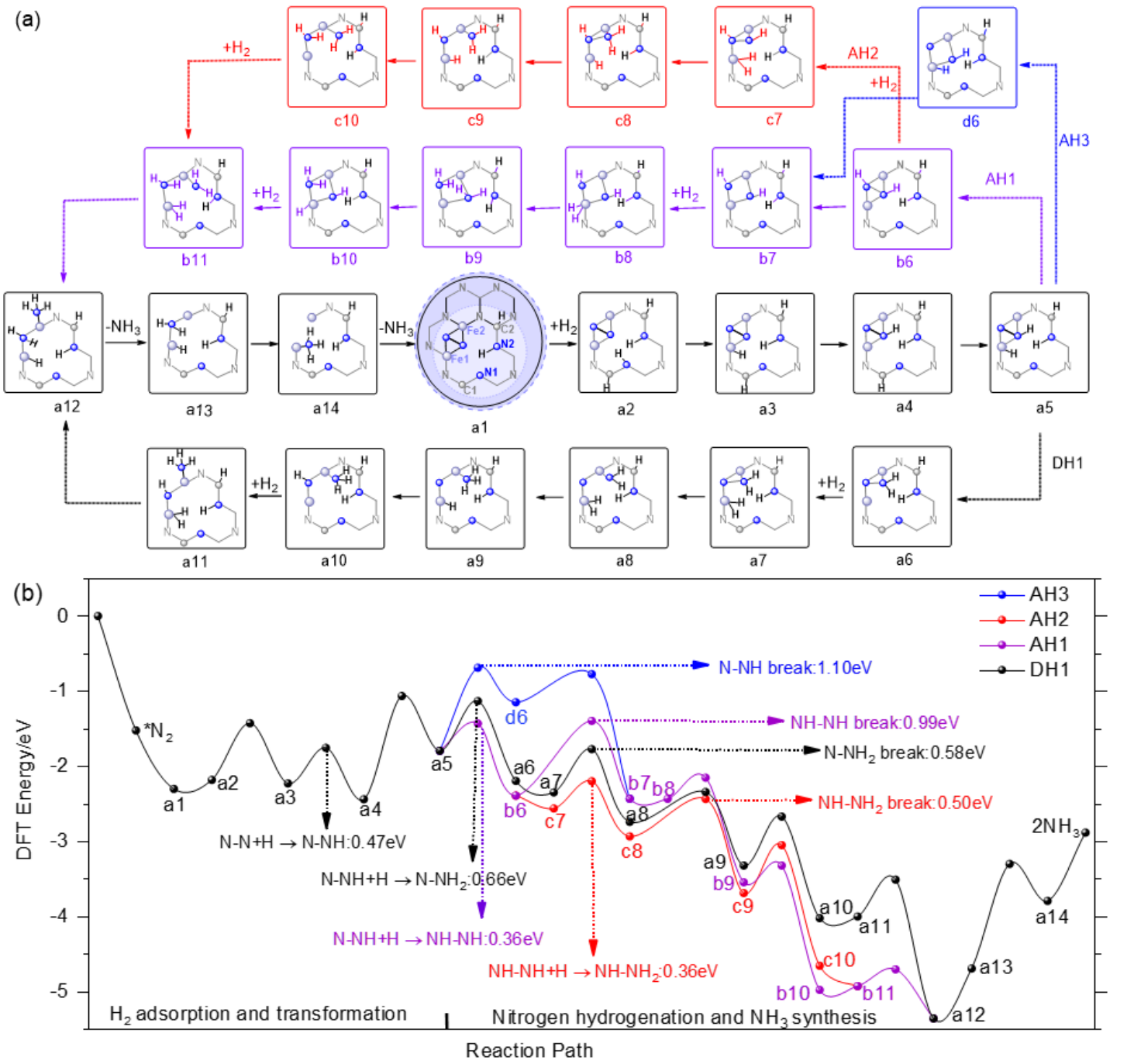

Figure 2

(a) Schematic diagram and (b) Reaction energy diagram of four different synergistic associative hydrogenation mechanisms for conversion of N2 to NH3 catalyzed by Fe2/mpg-C3N4 clusters. (AH and DH are abbreviations for Alternate and Distal Hydrogenation, respectively.)

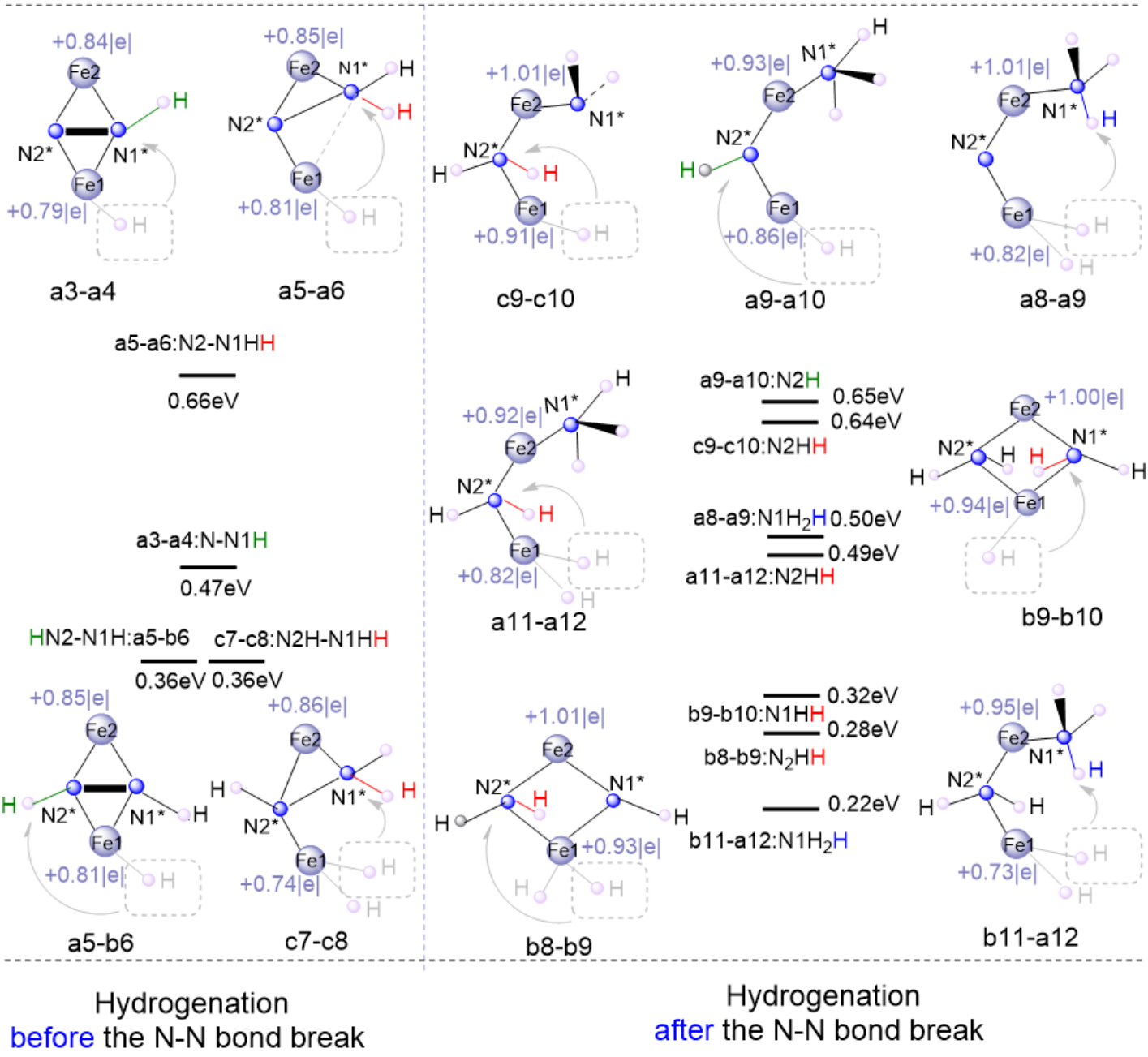

Figure 3

The N-H bond formation energy barriers in all hydrogenation mechanisms. (The hydrogen transferred on –N, -NH, and –NH2 is labeled green, red and blue, respectively).

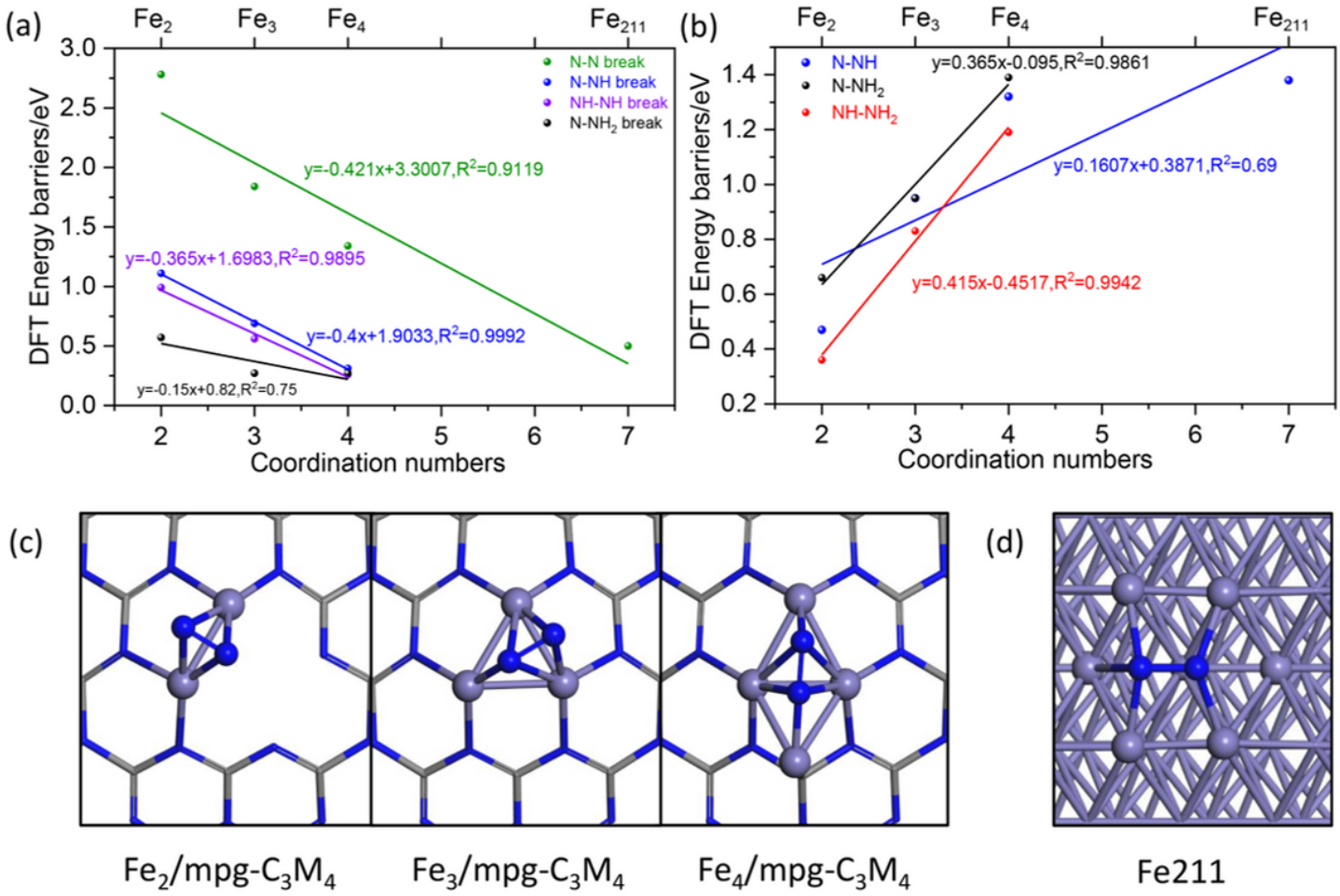

Figure 4

The N-N bond dissociation (a) and N-H bond formation (b) energy barrier correlation with Fe coordination numbers in *NHxNHy (x=0-1, y=0-2); The corresponding N2 adsorption configurations in Fen/mpg-C3N4 (c) and Fe(211) surface (d).

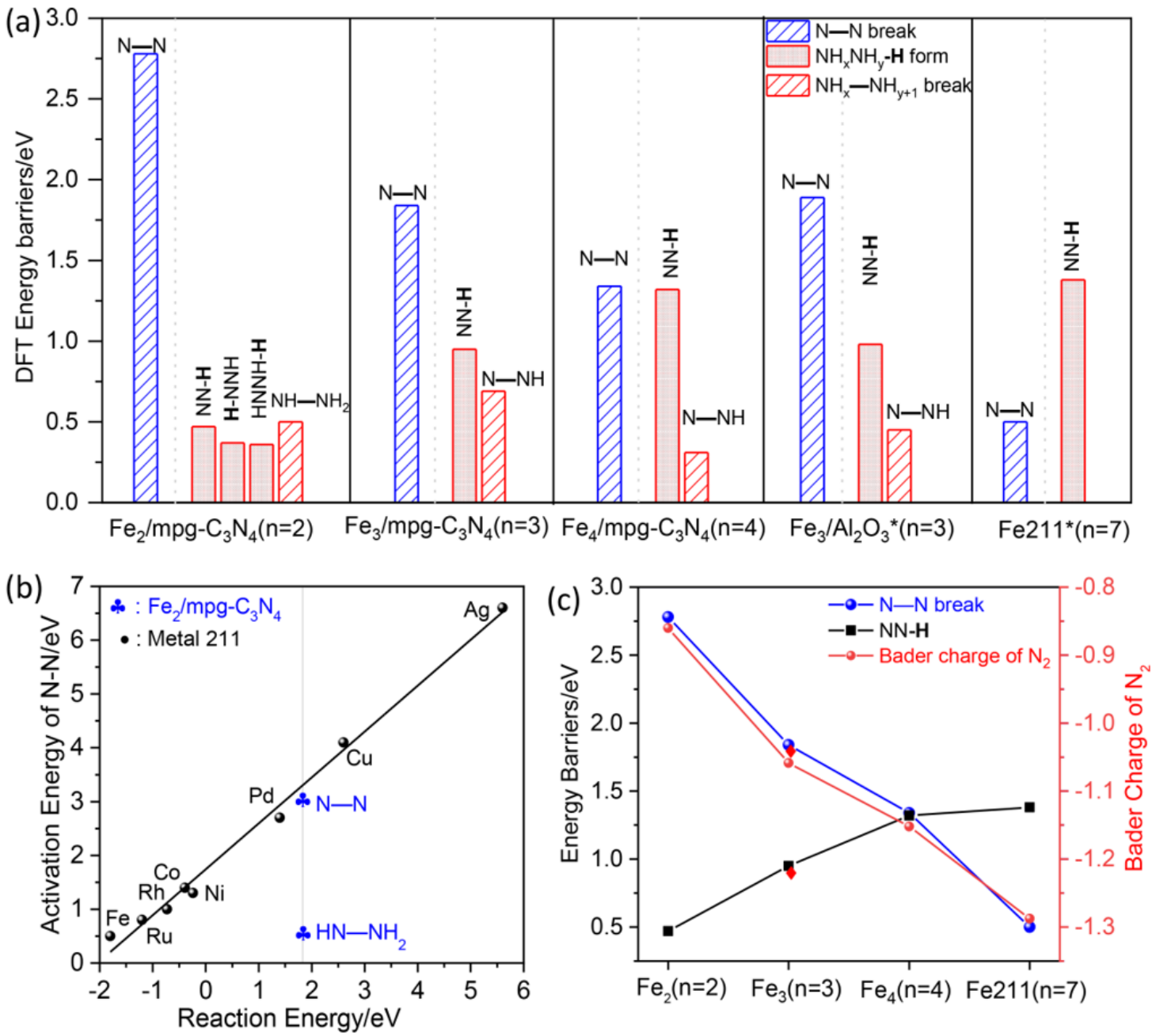

Figure 5

(a) Key energy Barriers of preferred reaction pathway on different Fen clusters (Fen/mpg-C3N4 (n=3,4), Fe3/Al2O3) and Fe (211); (b) The activation energies of N-N bond dissociation as a function of the Nitrogen dissociation reaction energy over step sites on Fe, Ru, Rh, Co, Ni, Pd, Cu and Ag surfaces; (c) The relationship of N2 dissociation and N2 hydrogenation energy barriers with the corresponding *N2 Bader charge. (The DFT energy barriers for Fe3/Al2O3 and Fe (211) in figure (a) from ref 19 and The energy data for the metal surfaces in (b) are taken from ref 53, 54)

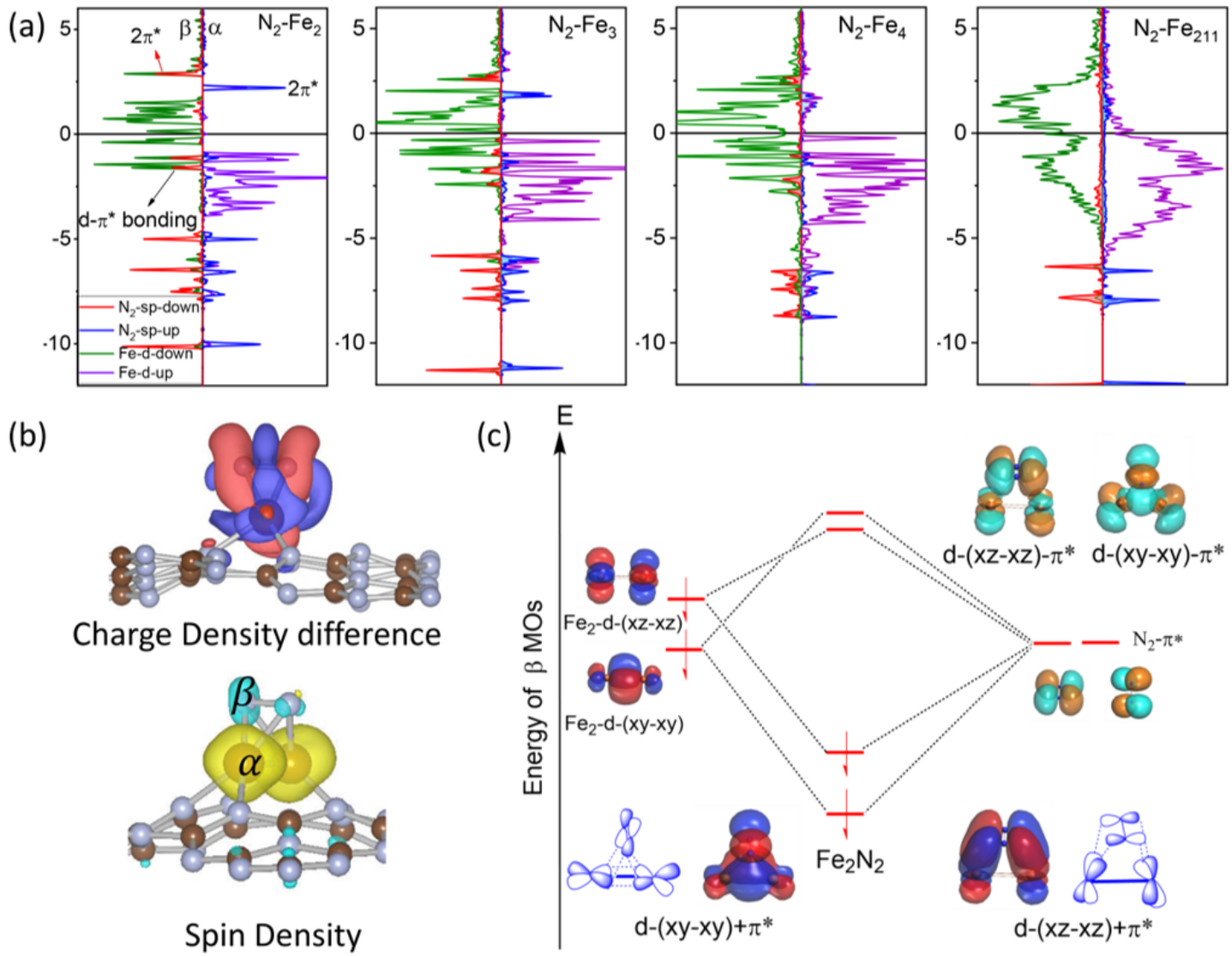

Figure 6

Electronic structure analysis of nitrogen adsorption. (a) Projected electronic density of states (PDOS) of the interaction between N2 and Fen clusters (The spin-polarized DOS of Fe-d-up, Fe-d-down, N2-sp-up and N2-sp-down are in purple, green blue and red respectively.); (b) Spin density (yellow stands for spin up and cyan for spin down) and Charge density differences (δρ=ρ(A+B)-ρA-ρB, charge depletion and accumulation regions are in light purple, blue and red, respectively) of N2 adsorption on Fe2/mpg-C3N4; (c) The major interactions and energy levels of the scalar relativistic Kohn–Sham β-spin MOs of isolated Fe2N2 with correlation to the orbitals from Fe2 and N2 fragments.

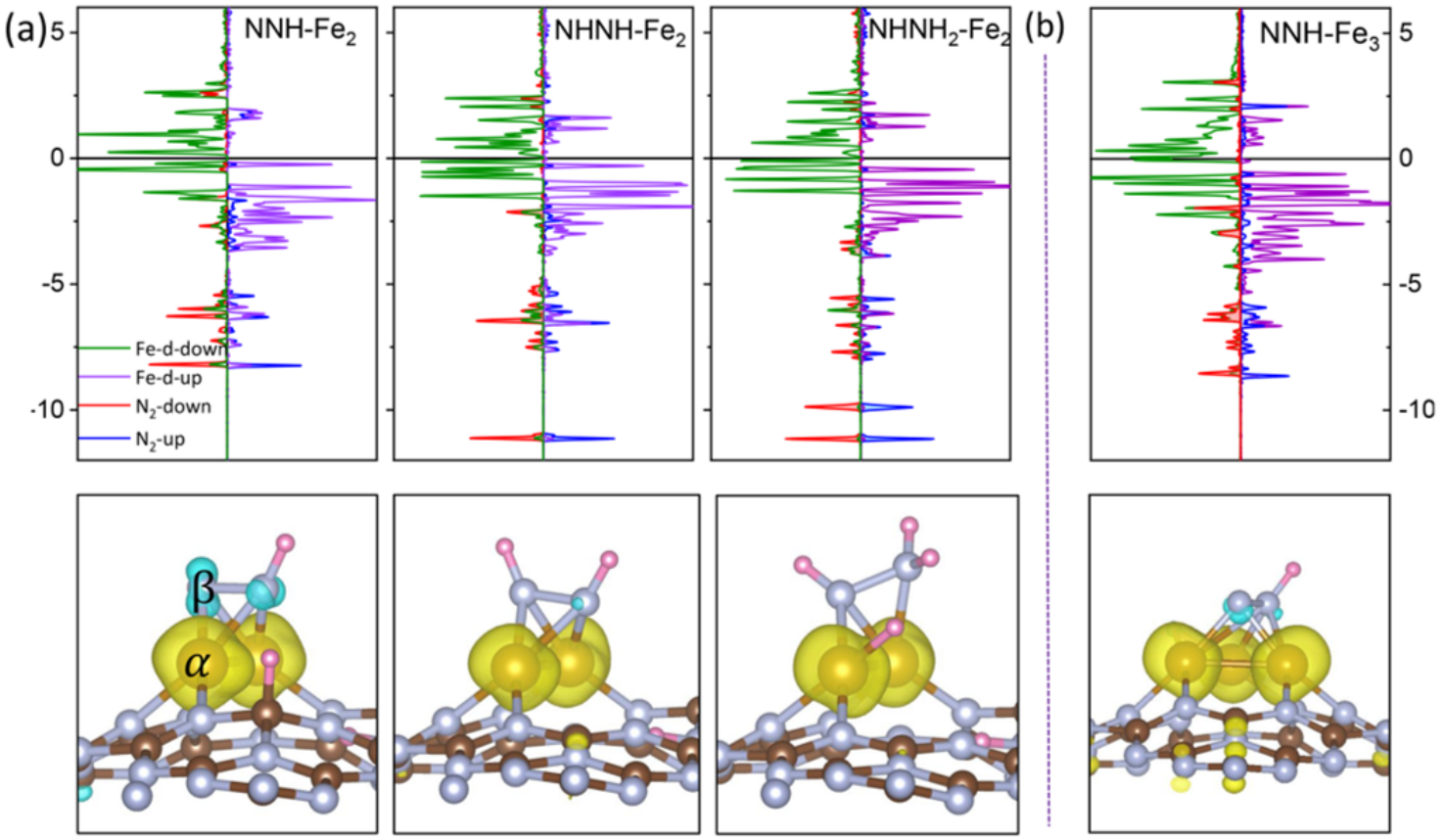

Figure 7

(a) Projected electronic density of states (PDOS) of NHxNHy species and corresponding spin density in Fe2/mpg-C3N4; (b) Projected electronic densities and spin density of *NNH in Fe3/mpg-C3N4.

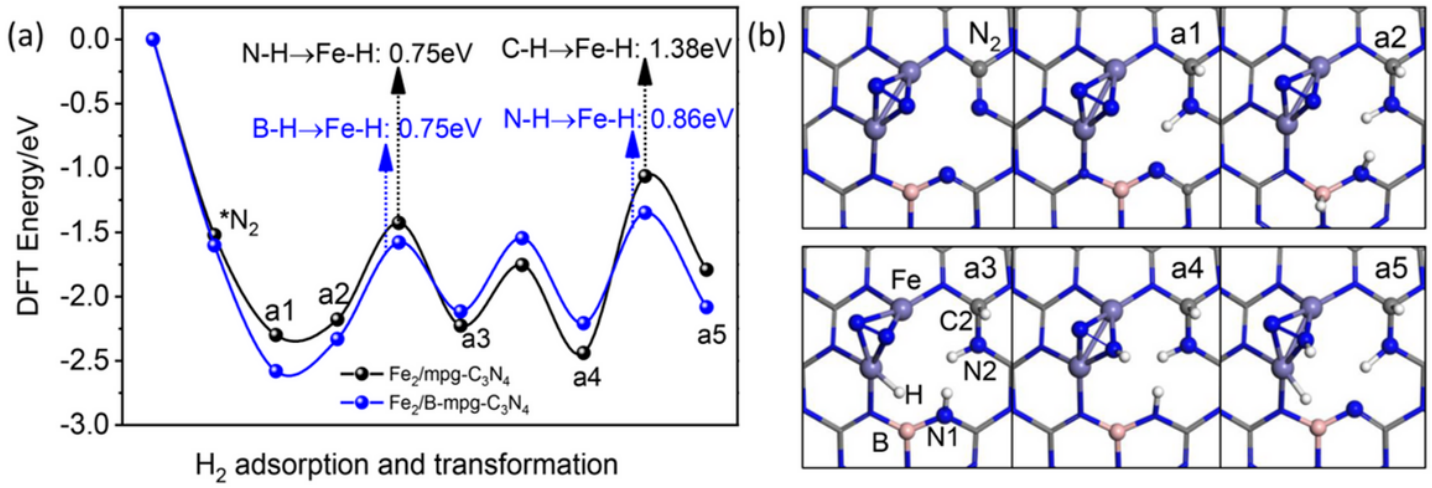

Figure 8

(a) The reaction pathways for the activation and transformation of Hydrogen on Fe2/mpg-C3N4 and Fe2/B/mpg-C3N4; (b) The corresponding structures on Fe2/B-mpg-C3N4.

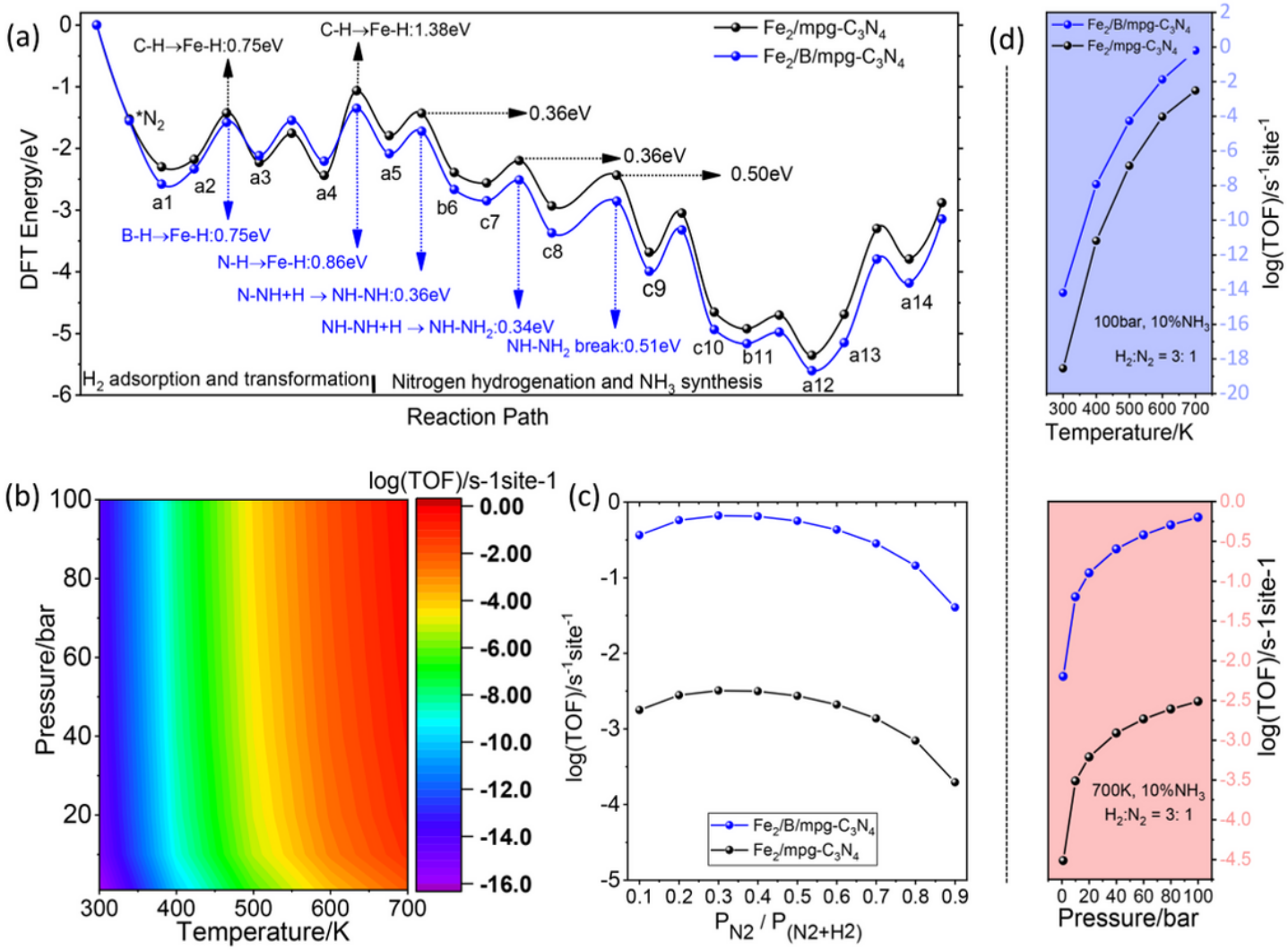

Figure 9

(a) Energy diagrams of optimal associative mechanism for ammonia synthesis on Fe2/mpg-C3N4 and Fe2/B/mpg-C3N4; (b) TOF per site of ammonia synthesis on Fe2/B/mpg-C3N4 mapped with pressure (1–100 bar) and temperature(300–700K). (c) TOFs per site of ammonia synthesis as a function of N2 partial pressure at 700 K and 100 bar; (d) TOF contributions at constant pressure of 100 bar and constant temperature of 700 K, respectively.

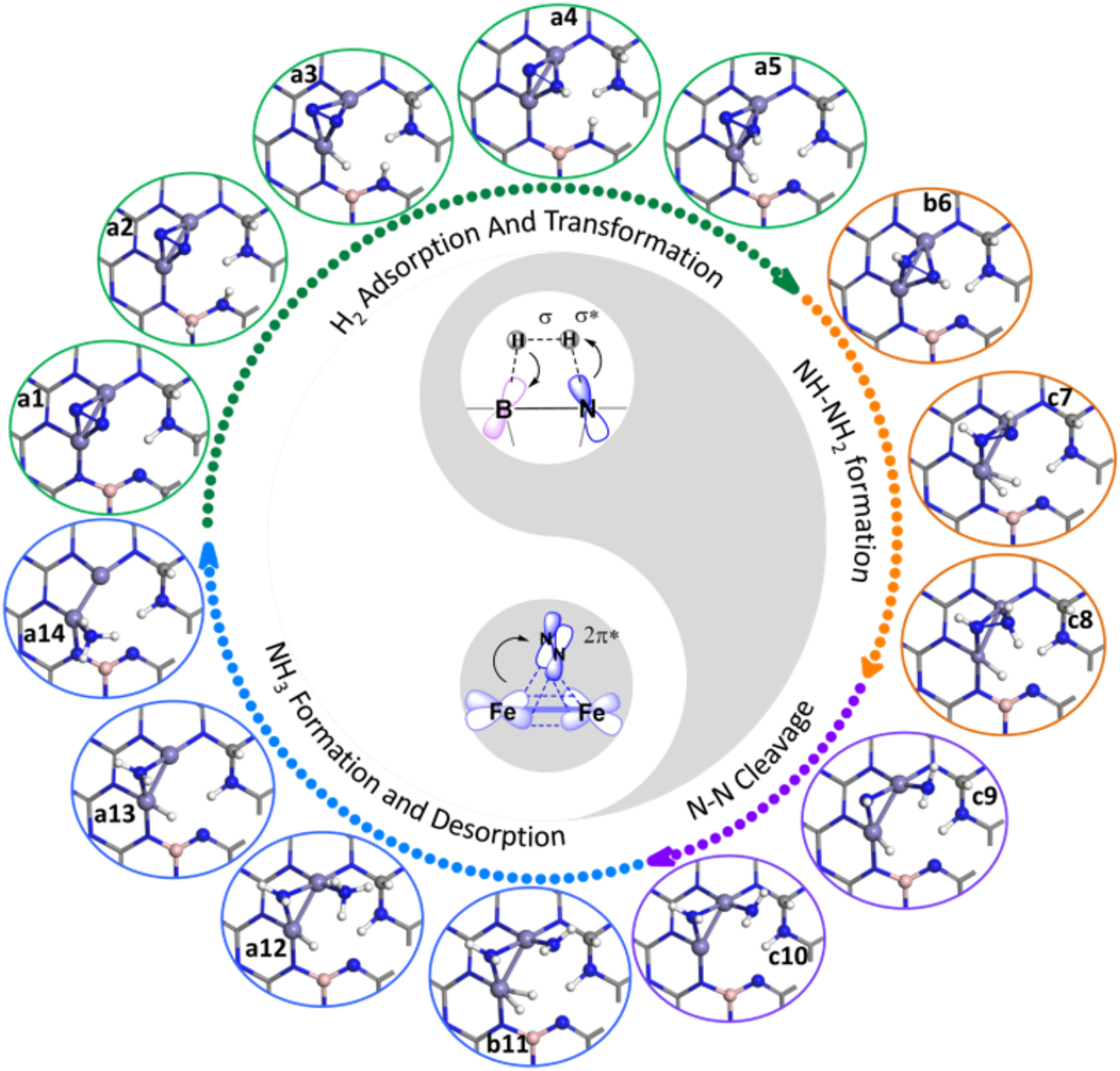

Figure 10

Catalytic Cycle Diagram of preferred reaction pathway for the thermal conversion of N2 to NH3 on Fe2/B/mpg-C3N4.

Supplementary Files

This is a list of supplementary files associated with this preprint. Click to download.

- TOC.png
- Scheme1.png
- 2021312SupportingInformationNC.docx